# Numerical modelling of wave interaction with coastal structures

## dr ir Peter Troch

Afdeling Weg-& Waterbouwkunde, Vakgroep Civiele Techniek TW15
Universiteit Gent, Technologiepark 904, 9052 Zwijnaarde
Tel: 09/264 54 89   Fax: 09/264 58 37   Email: PeterB.Troch@UGent.be

**Abstract**

The classic approach of studying the wave interaction with coastal structures is performing physical model testing on a scaled model of the structure in a wave flume in the laboratory. During the last decade, numerical modelling has become a powerful and efficient research tool in the field of coastal engineering. In this paper the numerical model VOFbreak[2], based on the Navier-Stokes equations and the Volume-Of-Fluid (VOF) technique for treating free surfaces, is presented which is capable of simulating the wave propagation and interaction with a variety of coastal structures. Two practical test cases illustrate features, advantages and limitations of the numerical model. In the first test case, wave propagation into a porous rubble mound breakwater and attenuation of the induced pore pressures is investigated. The second test case presents simulations of wave run-up and overtopping at an impermeable sea dike.

## 1 Introduction

Coastal zones typically have high densities of population, and important harbours with intense economic activities are located along the coastlines. Usually coastal structures, such as sea dikes, breakwaters, quay walls, jetties, etc… are constructed to protect people and harbour activities against large waves and flooding from storm surges. In this paper two types of coastal structures will be looked at in more detail: the rubble mound breakwater and the sea dike. Both types are well-known coastal structures in Belgium and the Netherlands.

Traditionally, the design of coastal structures such as breakwaters and dikes is based on small scale physical modelling. A scaled model of the structure (typically on a scale between 1/20 to 1/50) is subjected to the loading from high water level and large waves in a physical wave flume. Due to the complexity of both the loading (wave characteristics) and the structural characteristics, physical modelling was the appropriate design tool. Since the early seventies, a 'new' design tool developed simultaneously with the progress of computer performance: the use of numerical modelling.

The use of physical scale models has the advantage that the physical (mostly very detailed and complex non-linear) processes are inherent in the physical model, and can be easily reproduced. In a numerical model, all the processes have to be identified beforehand, and have to be built-in correctly inside the numerical code. At this stage, not all processes have been described adequately for use in the numerical models. Water flow is accurately simulated, but e.g. stability of armour units cannot yet be studied in the numerical flume.

Also, due to time-constraints (cpu time), only the most important processes are solved in the numerical codes, and assumptions and simplifications are a major part of the simulation. The physical model allows a direct visualisation of the flow, allowing a proper and accurate physical understanding of the flow and the structural behaviour.

Numerical models on the other hand have the advantage that less man power is required for execution of the tests. Once the numerical model has been calibrated using physical model results, the numerical model is more suitable for comprehensive parametric studies which require a lot of test repetition. Parameters which are difficult to measure in the physical wave flume, may be easily derived from the numerical calculation results (e.g. the velocity field spatially distributed over the whole computational domain, or the pressure distribution along a wall). Numerical simulations are useful during preparation of complex physical model tests, e.g. in selecting the most efficient model orientation and model dimensions for the required wave loading, or e.g. by predicting the expected flow characteristics.

Today the struggle between both types of models seems to be pacified. Indeed, only a synergy and integration of both tools into the design process will lead to the best design result. By combining the advantages of both models, an interaction grows between the two tools that will lead to an improved evaluation of the governing physical processes and eventually to an optimised design of the coastal structure.

This paper provides an overview of the potential of the numerical model VOFbreak², developed at Ghent University, which can be used as a numerical wave flume for studying the interaction between waves and a structure. First the numerical model itself with the governing equations will be shortly presented in section 2. The key innovations in the numerical wave flume that are necessary for simulation of wave interaction with permeable and impermeable coastal structures are a porous flow model, and wave boundary conditions for generation and absorption of the waves. Two practical test cases will illustrate the present possibilities and limitations of the code. First the attenuation of wave induced pore pressures inside the core of a porous rubble mound breakwater at Zeebrugge will be studied in section 3. Section 4 presents results on wave overtopping over an impermeable sea dike. Both types of structures have been built along the Belgian coast. Finally in section 5 conclusions are drawn and a personal view on future developments is given.

## 2 The numerical model VOFbreak[2]

### 2.1 The hydrodynamic flow solver

The numerical wave flume VOFbreak[2], <u>VOF</u>-algorithm for <u>break</u>ing waves on <u>break</u>waters, is based on the original SOLA-VOF code (Nichols et al., 1980) and the RIPPLE code (Kothe et al., 1991) capable to compute free surface flow when the fluid domain becomes multiply connected. Incompressible Newtonian fluid with uniform density is assumed in the vertical plane (two-dimensional), governed by the Navier-Stokes equations:

$$\frac{\partial u}{\partial t} + u\frac{\partial u}{\partial x} + v\frac{\partial u}{\partial y} = -\frac{1}{\rho}\frac{\partial p}{\partial x} + \nu\left(\frac{\partial^2 u}{\partial x^2} + \frac{\partial^2 u}{\partial y^2}\right) + g_x \tag{1}$$

$$\frac{\partial v}{\partial t} + u\frac{\partial v}{\partial x} + v\frac{\partial v}{\partial y} = -\frac{1}{\rho}\frac{\partial p}{\partial y} + \nu\left(\frac{\partial^2 v}{\partial x^2} + \frac{\partial^2 v}{\partial y^2}\right) + g_y \tag{2}$$

and the continuity equation:

$$\frac{\partial u}{\partial x} + \frac{\partial v}{\partial y} = 0 \tag{3}$$

where t (s) is time, u and v (m/s) are the velocity components in x and y direction respectively., p (N/m²) is pressure, and $g_x$, $g_y$ (m/s²) are horizontal and vertical gravity components respectively, ρ (kg/m³) is the density of the water, ν (m²/s) is the kinematic coefficient of viscosity.

The free surface is described by introducing a function F(x, y, t) that represents the fractional volume of fluid in the mesh cells. The volume of fluid evolution equation (4) expresses that the volume fraction F moves with the fluid:

$$\frac{\partial F}{\partial t} + u\frac{\partial F}{\partial x} + v\frac{\partial F}{\partial y} = 0 \tag{4}$$

Finite difference solutions of the four unknowns u, v, p and F, are obtained on an Eulerian rectangular mesh in a Cartesian co-ordinate system (x,y). The volume of fluid function F, defining the fluid regions, is updated using the donor-acceptor flux approximation for the calculation of fluxes from a donor cell to an acceptor cell. A unit value of F corresponds to a full cell, while a zero value indicates an empty cell. Cells with values between zero and one and having at least one empty neighbour cell contain a free surface. A line is constructed in each surface cell with the correct calculated surface slope and correct amount of fluid lying on the fluid size, and is used as an approximation to the actual free surface. In the current version a constant eddy viscosity turbulence model is used.

The code is implemented on a UNIX workstation using ANSI C, providing general computer compatibility, and providing a flexible code structure for adaptations with little effort. A series of post-processing tools has been developed for the visualisation, processing and interpretation of the computed results. Numerical instrumentation for the acquisition of relevant phenomena (wave height, run-up level, pore pressure, surface elevation, ...) is included for easy access to calculated data. A complete description of the underlying mathematical model, the details of the governing equations and the solution algorithms is available in Troch (2000).


**2.2 Porous flow and wave boundary conditions**
A number of extensions have been implemented into the code in order to allow the simulation of the wave interaction with a rubble mound breakwater and a sea dike.

**2.2.1 Porous Flow Model**
The governing Navier-Stokes equations are extended, to include the simulation of porous flow inside the permeable core of the breakwater, using Forchheimer flow resistance terms. The Forchheimer porous flow model, as an extension to the well-known Darcy model in groundwater flow, takes into account the turbulent flow contribution which –for the case of rubble mound breakwaters– is larger than the viscous contribution to the flow resistance.

**2.2.2 Wave Boundary Conditions**
A number of wave boundary conditions are implemented. Incident waves are generated using boundary wave generation. Linear wave theory is applied at the boundary of the computational domain to provide the surface elevation and the velocity components of the incident wave at the boundary. For absorption at the boundary of reflected waves, the active wave absorbing technique AWAVOF is used (Troch and De Rouck, 1999). This new

numerical boundary condition is based on an active wave absorption system that is well known already for physical wave flume application using a wave paddle. Velocities are measured at one location inside the computational domain. The reflected wave train is separated from the incident wave field in front of the structure by means of digital filtering and subsequent superposition of the measured velocity signals. This way an additional incident wave train is determined in order to absorb the reflected wave train. The AWAVOF method is optimised for efficient use in a numerical wave flume and applies to regular and irregular waves.

These modifications allow the numerical modelling of the wave induced pore pressure attenuation inside a breakwater core as presented in the next section. The detailed description of the theoretical background and the implementation of the modifications are reported in Troch (2000).

## 3 Attenuation of pore pressures inside the Zeebrugge rubble mound breakwater

### 3.1 Pore pressures inside a rubble mound breakwater

A typical design cross section of a rubble mound breakwater is shown in Fig. 1. The core is made of rock and constitutes the main part of the breakwater. The porous flow inside the permeable core is caused by the waves and experiences high energy dissipation due to friction losses. An armour layer of individual heavy concrete blocks protects the core from the waves. A toe at the sea bottom acts as a foundation for the armour layer. A filter layer between the core and the armour layer also acts as foundation layer for the armour layer, and prevents that the fine rock in the core is washed out in between the holes of the armour layer.

The interaction between the waves and the breakwater is described by a large number of related physical processes. As an example, the breakwater at Zeebrugge in Belgium is shown during storm conditions (Fig. 2). Waves propagate towards the breakwater and run up and down the armour layer. Part of the wave energy is reflected back to the sea, part of the energy is dissipated in the armour and filter layer and in the core, the remaining part is transmitted through the breakwater. The porous flow inside the core has both laminar and turbulent flow characteristics and is connected to the wave attack via infiltration and seepage through the armour layer. The hydrodynamic pore pressures associated with the porous flow (i.e. the wave induced water pressure inside the holes of the skeleton of the rock material) decrease with increasing distance from the seaward slope. Harlow (1980) reports a number of recent failures of rubble mound breakwaters during storms and concludes that in most cases the failure is caused by very large pore pressures in the breakwater core. De Groot et al. (1994) present the importance of the knowledge of the pore pressures in the design of a breakwater, in particular for the slope stability analysis, for the design of filter constructions near the bottom of the breakwater, and for the influence of pore pressures on hydraulic stability of armour units, on wave run-up and overtopping, on wave transmission and on internal set-up of the phreatic water table. The exact knowledge of the pore pressures therefore is very important for a stable and safe breakwater structure. However it is very difficult to estimate the magnitude of the pore pressures accurately. Due to the complexity of both wave loads and structure itself there are no analytical expressions available. In conventional small scale model tests (scale ranging between 1:30 till 1:70) viscous scale effects influence the porous flow inside the breakwater core adversely. A numerical simulation of the pore pressure attenuation inside the breakwater core provides an alternative answer to this problem.
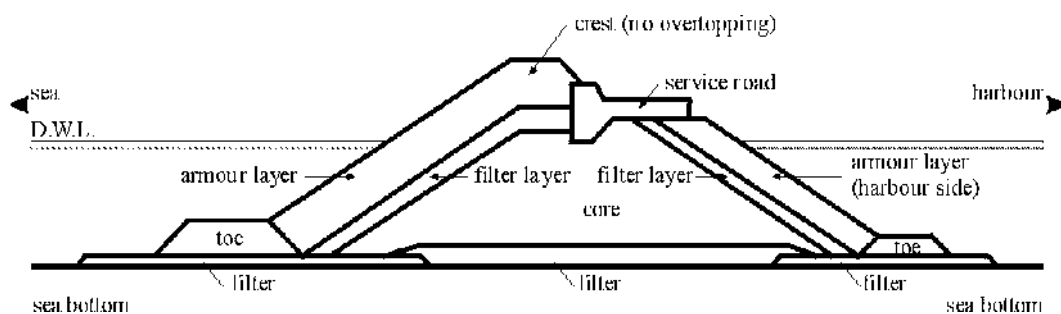
**Fig. 1.** *Typical cross section of a rubble mound breakwater (no overtopping conditions).*



**Fig. 2.** *Photo of wave interaction with the Zeebrugge rubble mound breakwater during storm conditions (significant wave height estimated around 3 meters).*

Before the numerical simulation of the wave interaction is started, a detailed validation process has been carried out using physical model data. The results from this validation are described briefly in the next section.

### 3.2 Validation of numerical wave flume using physical model tests
Physical model test data have been acquired in a wave flume at Aalborg University (Denmark) for the validation of the wave interaction with a breakwater. The test set-up included a relatively simple breakwater lay-out with a vertical front wall and a core of homogeneous rock (porosity n = 0.426, mean grain size $d_{50}$ = 0.0181 m), Fig. 3.
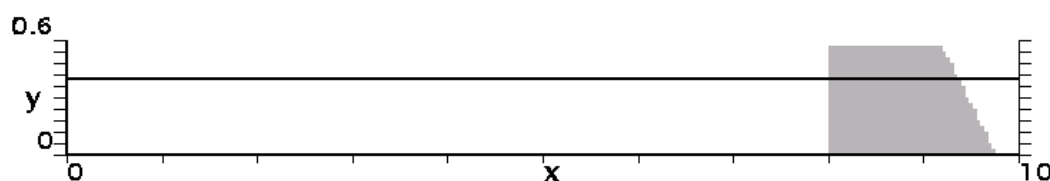


**Fig. 3.** *Geometry of the wave flume set-up, with wave generation and absorption at the left boundary (x = 0) and the breakwater near the right boundary.*

The validation process aims at comparing the reflection, run-up, transmission and pore pressures from both the physical model and the numerically simulated equivalent model for the same geometry, material characteristics and wave conditions. In this section, only a comparison with respect to the pore pressures will be discussed. A comparison for the other processes is available in Troch (2000).

The numerically calculated pore pressures inside the core are compared with the pore pressure measurements from the physical model at five positions on two horizontal levels. Fig. 4 shows an example of the validation results for one test (reg10h), at two horizontal levels at a depth y' below SWL respectively, for incident regular waves (H = 0.06 m, T = 1.80 s). In this case the viscous friction term is neglected and only turbulent friction losses are accounted for in the Forchheimer porous flow resistance model.
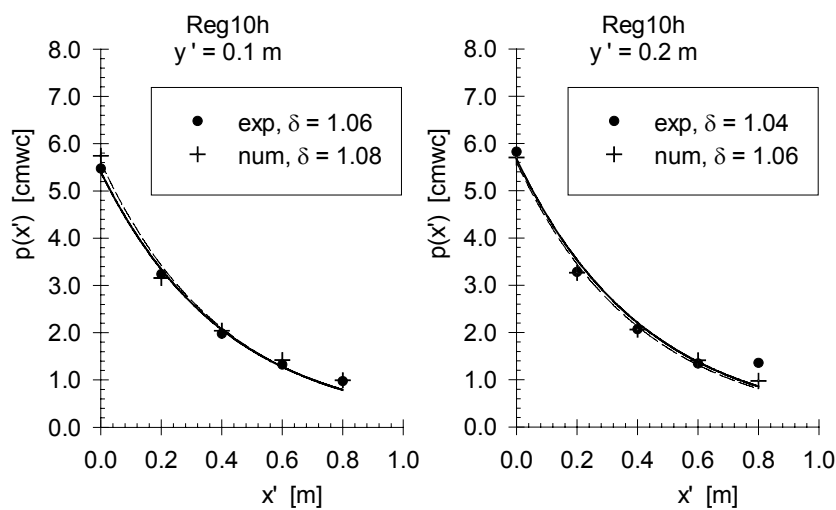


**Fig. 4.** *Distribution of pore pressure heights* p(x') *versus position* x', *for two levels at resp. depth* y' *= 0.10 m and* y' *= 0.20 m, calculated from physical model tests (exp) and numerical simulations (num) resp., for test reg10h.*

The solid and dashed lines in Fig. 4 indicate a fitted exponential damping model (5) through the experimental and the numerical data respectively, from where the damping coefficient $\delta$ is obtained and plotted in Fig. 4. The exponential damping model for the attenuation of the pore pressure height is:

$$p(x) = p_0 \exp(-\delta \frac{2\pi}{L'} x) \qquad (5)$$

where x is the co-ordinate across the core (m), where x = 0 at the interface between filter layer and core; $p(x)$ is the pore pressure height at position x (kPa); $p_0$ is the reference pore pressure height at x = 0 (kPa), L' is the wave length within the breakwater (m), $\delta$ is a damping coefficient (-). The wave length within the breakwater L' is calculated from $L' = L/\sqrt{1.4}$, where L is the wave length. The pore pressure height $p(x)$ is the envelope function of the instantaneous pore pressures $p(x, t)$ along the x-axis. A detailed discussion of the damping model (5) is provided in Troch et al. (2003).

It is clear from Fig. 4 that very good agreement is found between the physical model test data and the numerically calculated data. From these results (in fact from a much more detailed validation analysis, see Troch, 2000) it is concluded that the numerical model VOFbreak[2] is capable of simulating the wave interaction with a simple breakwater.


### 3.3 Numerical modelling of wave interaction with breakwater

Finally, the Zeebrugge prototype breakwater is tested in the numerical wave flume VOFbreak[2]. A number of approximations have been used. The bathymetry in front of the breakwater is simplified by using a constant water depth d = 8.0 m. The incident waves are regular waves with wave height H = 3.0 m and wave period T = 8.0 s. The AWAVOF wave absorption system is switched on. The considerable energy dissipation in the armour and filter layers is modelled by using a layer on top of the breakwater core with higher permeability than the core material.

Fig. 5 shows the numerical set-up with the wave generation/absorption system AWAVOF at the left boundary (x = 0 m) and the Zeebrugge breakwater with simplified geometry near the other boundary. At the right boundary (x = 160 m) a passive wave absorption system is installed. The simulation is started from still water conditions. The cell dimensions are $\Delta x$ = 0.50 m and $\Delta y$ = 0.40 m in x and y-direction resp., resulting in 323 x 43 cells for the complete computational domain. The total simulation time is set to 200 s with a time step of $\Delta t$ = 0.005 s. The calculations took 4 hours on a Pentium III PC.

Fig. 6 shows the resulting free surface position in front of the breakwater, in the armour layer and in the core from the simulation at t = 122 s (run-down) and t = 127 s(run-up). Inside the armour layer the energy dissipation of the wave action and the damped movements of the free surface are observed. The variation of the water level in the core is even more attenuated resembling the working principle of a breakwater.

In Fig. 6 only information from the time instant of the two 'snap-shots' is available. It is relatively easy to visualise the numerical results during a complete wave period in order to increase the information that is calculated. In Fig. 7 the results from the calculations (pressure p, and velocity components u and v) are given for a cycle of one wave period. Instantaneous values at t = (i/9)T (i = 1, 2, ..., 8) and envelope values of pressure and velocities along the x-axis are presented. The data are taken from the horizontal level located one wave height below the still water level, and are given for the foreshore area (left column) and for the breakwater area (right column). In the graphs of the right column, the x-axis has been stretched for better visualisation. Also, the u- and v-axis in the right column have been stretched (factor 2) for better visualisation. The hatched area is the area inside the armour layer. From these graphs in Fig. 7 it is seen that both pressure and velocities attenuate inside the armour layer and even more in the breakwater core.
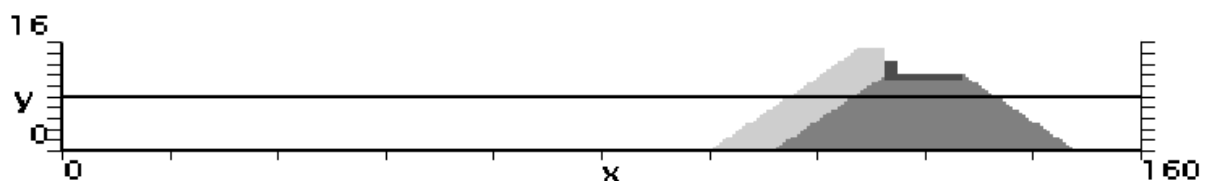


**Fig. 5.** *Geometry of the numerical wave flume set-up, with wave generation at the left boundary and the Zeebrugge breakwater near the right boundary.*

This physical behaviour is comparable to the prototype processes. The pore pressure amplitudes decrease exponentially towards the backward slope where the pore pressure is almost zero. Maximum velocities (both u and v) inside the core are about 0.25 m/s close to the slope and decrease gradually to 0 m/s near the backward slope. The horizontal velocity u in the volume of water running up and down the slope is about two times higher than the vertical velocity at the same location. This indicates that infiltration and seepage processes predominantly act in horizontal direction.

Finally in Fig. 8 a snap-shot of the detailed calculated flow field in the zoomed area around the breakwater slope is given for the case of wave run-up at t = 127 s. Fig. 8 shows the velocity vector field, the isobars and the position of the free surface. It is clearly perceptible that during wave run-up both infiltration (near the free surface) and seepage (near the bottom) occur at the same time along the slope. The wave interaction therefore cannot be reduced to one dimension.

Detailed analysis of the resulting pore pressure field with regard to the applicability of the damping model (5) shows that the numerical model is capable to predict the pore pressure attenuation accurately (Troch, 2000).
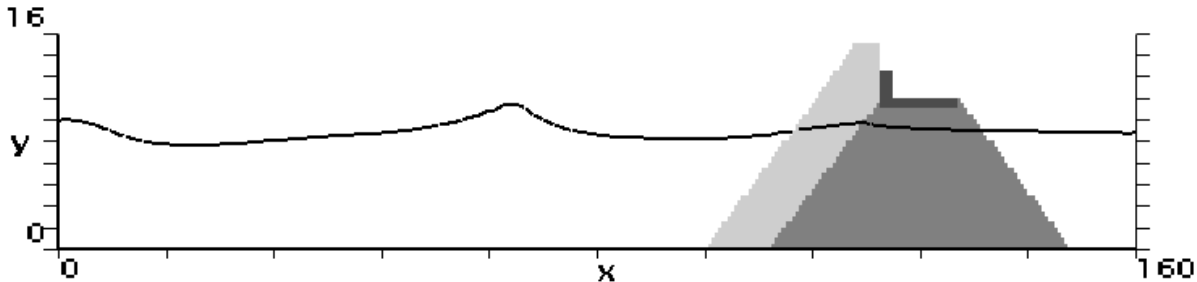
*(a) wave run-up at t = 122 s*
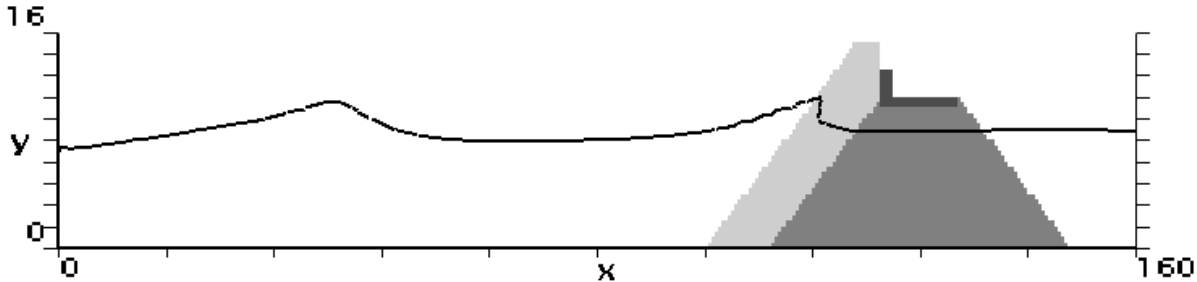
*(b) wave run-down at t = 127 s*

**Fig. 6.**  *Results from numerical simulation with Zeebrugge breakwater at t = 122 s and t = 127 s, showing the free surface in front of the breakwater, in the armour layer and in the core (distorted scale in y direction using factor 2).*
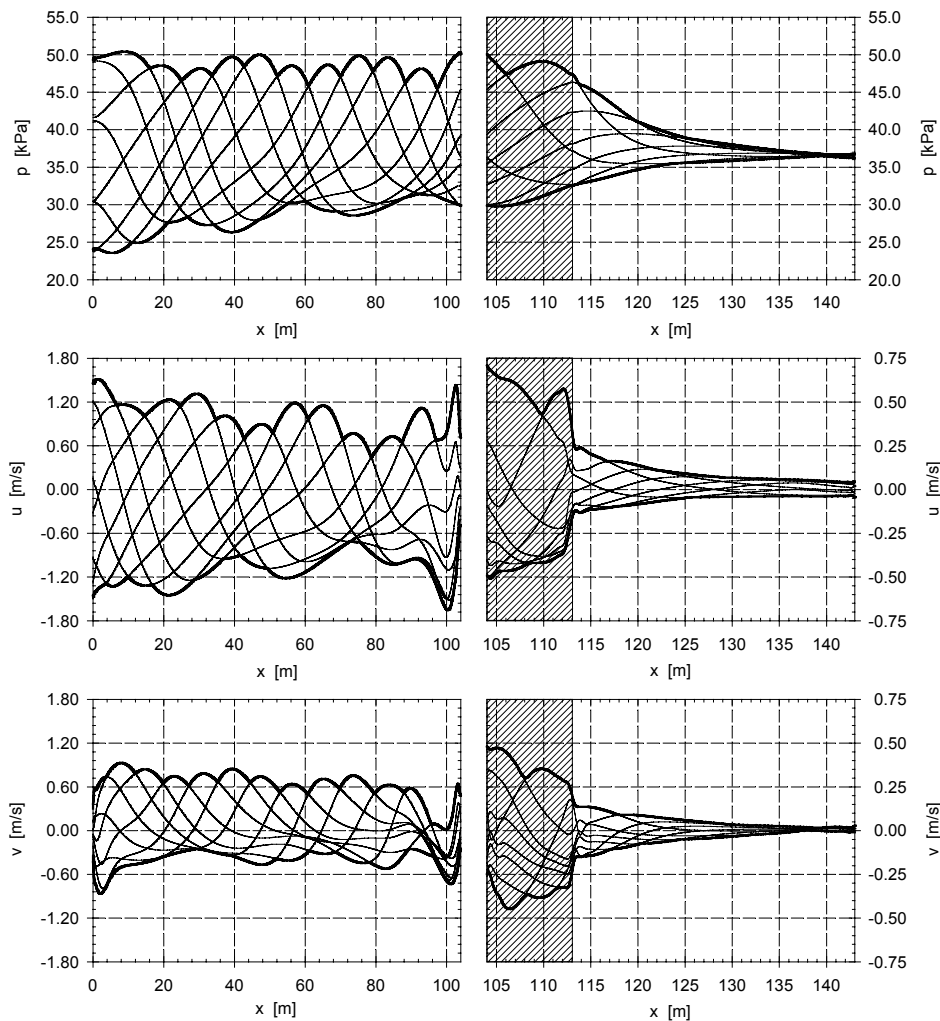
**Fig. 7.** *Calculated instantaneous values of pressure p and velocities u, v (and envelopes) vs. position x located one wave height below the still water level, for 8 consecutive time instants during one wave period between t = 120 s and t = 127 s. Left column is for the foreshore area (water), right column is for the breakwater area (armour layer - hatched area- and core material).*
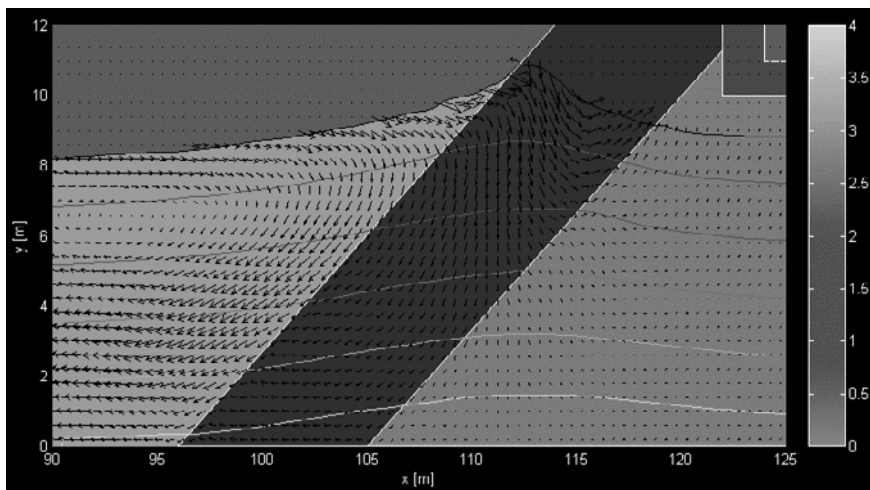


**Fig. 8.** *Calculated flow field near the breakwater slope during wave run-up at t = 127 s.*

## 4 Wave overtopping at an impermeable sea dike

### 4.1 Geometry of the impermeable sea dike

Dikes protect the coastlines of Belgium, The Netherlands, Germany, Denmark and Poland over several thousands of kilometres from waves and flooding. Therefore the correct design of these coastal structures is very important to avoid high costs, in both cases of overdesign and underdesign. In general the design is based on design storm surge levels and a 2% exceedance wave run-up. However wave overtopping has to be taken into account due to the remaining uncertainties in storm surge level and wave run-up. Physical model tests on a smooth impermeable sea dike have been performed recently (Oumeraci et al., 1999) in the wave flume of Leichtweiss Institut für Wasserbau (LWI, Germany). In this section, the results from numerical simulations of wave overtopping over the smooth sea dike, carried out using the numerical model VOFbreak$^2$ are presented and are compared to experimental data from the physical model.

Fig. 8 shows a typical example of a smooth impermeable sea dike during storm conditions, during a wave overtopping event. The geometry of the sea dike used for the simulations is shown in Fig. 9. The seaward (or outer) slope is 1:6, the landward (or inner) slope is 1:3. The crest height is 0.80 m. The crest and both slopes are impermeable and smooth to the external fluid flow. For the numerical simulations, the water depths d = 0.70 m, 0.75 m and 0.80 m have been used. The computational grid covers the area depicted in Fig. 9. The foreshore area is limited to 1.0 m. The height of the wave flume is 1.0 m. On the crest, two sections S1 and S2 are defined at the seaward (position x = 5.8 m) and landward side (x = 6.1 m) of the crest. These are used for calculation of the overtopping quantities (Fig. 10).

A non-uniform computational grid is generated, allowing to increase the grid resolution in areas where the fluid flow is complex (e.g. on the seaward dike slope where wave breaking occurs) or where the layer thickness of the water tongue is small (e.g. on the dike crest). Obstacles with arbitrary (even curved) boundaries are modelled using the "partial cell treatment", allowing cell-cutting boundaries. In the case of modelling the dike slopes, this approach avoids a staircase-slope approximation.



**Fig. 8.**  *A typical smooth impermeable sea dike during storm conditions.*
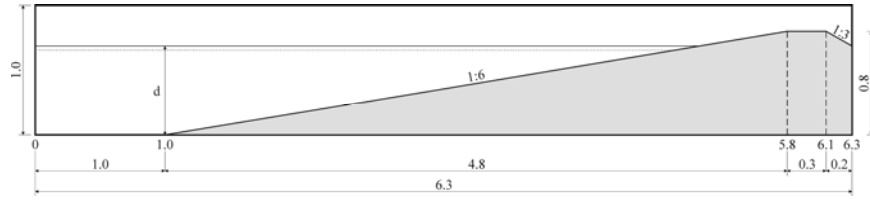
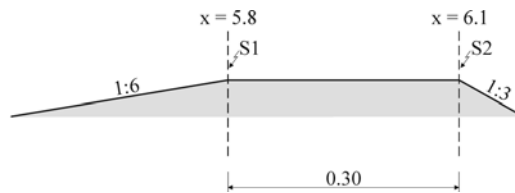**Fig. 9.** *Cross section of the sea dike cf. physical model tests at LWI.*



**Fig. 10.** *Detail of the dike crest, with sections S1 and S2 at seaward (position x = 5.8 m) and landward side (x = 6.1 m) of the crest, respectively.*

**4.2 Calculation of overtopping quantities and test programme**

A number of overtopping quantities are calculated from the numerical simulations. The direct solutions to the numerical calculations are the velocity components $u, v$ in horizontal and vertical direction, the pressure $p$ and the volume fraction $F$ in each cell of the computational domain. The instantaneous configuration of the free surface is reconstructed from the discrete mesh values of the volume fraction $F$. Velocities and pressure are available in discrete locations of the cells only. Using the information from these solved variables at each time step, the overtopping quantities such as layer thickness $h(t)$, instantaneous discharge $q(t)$ and cumulative overtopped volume of water $V(t)$ are derived in both sections S1 and S2. A detailed discussion of the derivation is given in Troch et al. (2002).

**Table 1.** *Test programme for numerical simulations of the 1:6 sea dike, including wave characteristics H and T, water depth d, surf similarity parameter $\xi_0$ and average overtopping rate $q_{lab}$.*

|  | Test No. | H [m] | T [s] | d [m] | $\xi_0$ [-] | $q_{lab}$ [l/sm] |
|---|---|---|---|---|---|---|
| 1 | **1** | 0.155 | 1.959 | 0.70 | 1.0 | **3.33** |
| 2 | **2** | 0.117 | 2.446 | 0.70 | 1.5 | **2.32** |
| 3 | **3** | 0.119 | 3.154 | 0.70 | 1.9 | **5.79** |

| | | | | | | |
|---|---|---|---|---|---|---|
| 4 | **4** | 0.121 | 4.150 | 0.70 | 2.5 | **8.59** |
| 5 | **2_75** | 0.117 | 2.446 | 0.75 | 1.5 | **7.51** |
| 6 | **2_80** | 0.117 | 2.446 | 0.80 | 1.5 | - |
| 7 | **2*_80** | 0.082 | 2.503 | 0.80 | 1.8 | **11.82** |

Table 1 includes, for each of the 7 selected tests, the wave characteristics (wave height $H$ and wave period $T$ for a regular wave), the water depth $d$, the surf similarity parameter $\xi_0 = 1/6 \Big/ \left(2\pi H / gT^2\right)^{0.5}$ and the average overtopping rate $q_{lab}$ as measured in the physical model tests at LWI. The seven tests will be referred to using the Test No. Tests 1, 2, 3 and 4 are four tests where the surf similarity parameter increases from 1.0 to 2.5 in steps of 0.5. Additionally the water depth is increased in tests 2_75, 2_80 and 2*_80 (note that for test 2_80 no physical model results are available) in order to study the influence of water depth and induced variation of overtopping volumes on the calculation results.


**4.3 Numerical modelling of wave overtopping over sea dike**

**4.3.1 Computational domain and boundary conditions**
At the left boundary ($x = 0$) the incident regular waves are generated using wave generation routines that are available in VOFbreak[2]. The bottom and top boundaries are modelled as free slip boundaries. The right boundary ($x = 6.3$) is modelled as free outflow boundary allowing the fluid to leave the computational domain without interaction with the wave run-up and overtopping processes. The non-uniform grid of the computational domain (Fig. 9) is composed of 160 x 28 cells with varying cell sizes : $\Delta x$ ranges from 0.020 m at $x = 5.5$ m to 0.060 m at $x = 0$ m; $\Delta y$ ranges from 0.020 m at $y = 0.70$ m to 0.056 m at $y = 0$ m. Using this set-up the highest resolution is obtained along the outer slope between the SWL and the crest, and on the dike crest itself. It is believed that these areas are most critical for accurate numerical calculations. The dike slopes and dike crests have been modelled as impermeable boundaries cutting through the cells, thus allowing a perfect representation of the dike slope.

**4.3.2 Plots of calculated free surface configuration**
Fig. 11 shows the typical result from a numerical simulation of the sea dike using VOFbreak[2], for tests 2, 2_75 and 2_80 (with increasing water depth), for a zoomed area near the dike crest (between $x = 4.0$ m and $x = 6.3$ m). The three plots show the free surface configurations (derived from the calculated volume fraction $F$) at $t = 9.0$ s. The wave running up the slope is clearly observed.
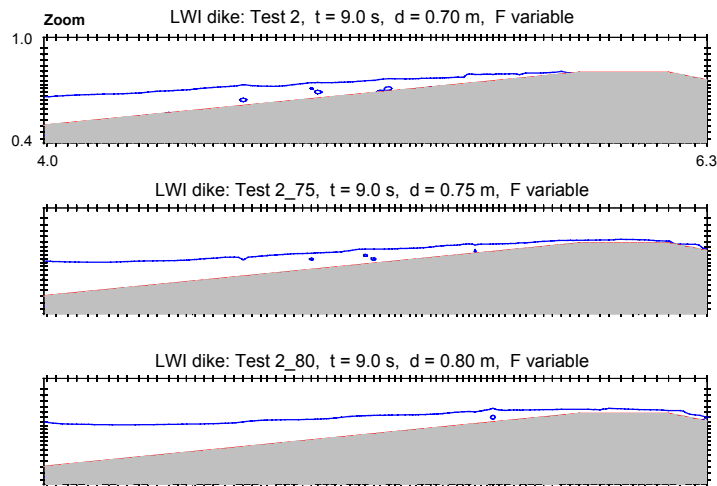
**Fig. 11.** *Free surface configurations (derived from volume fraction* F *) at time step* t = 9.0 *s, for a zoomed area near the dike crest, for three tests with increasing water depth.*

The voids in the up-running water tongue do not represent air bubbles in the breaking wave front. These voids are rather inaccuracies in modelling the free surface configuration for that highly turbulent flow area. A comparison of wave overtopping on the dike crest for test 2, 2_75 and 2_80 respectively, at t = 9.0 s is made. For higher water depths the layer thickness on the crest and the volume of overtopping water increases clearly. Fig. 11 illustrates that the physical processes of wave run-up and overtopping seem to be modelled in a realistic way. Quantitative validations using laboratory data will be carried out next.

### 4.3.3 Layer thickness and discharge

In both sections S1 (at x = 5.8 m) and S2 (at x = 6.1 m), layer thickness h(t) and instantaneous discharge q(t) have been calculated from the solved variables. A typical example of the resulting plot of time history of h(t) and q(t) is given in Fig. 12 for test 3. After one wave already (at t = 6.0 s) a reasonable regular pattern of wave overtopping is seen with a layer thickness of 0.07 m on average and a discharge of 0.02 $m^3$/sm on average, for section 1. At section 2 the regular pattern is not very clear, and although there is a clear correlation in time (time shift of the peaks at S2) both q(t) and q(t) may be underestimated. Comparison of cumulative overtopping volumes is required to conclude on this. The same regular pattern is present in most of the other tests as well and is acceptable as the transients from the "cold start" (from still water conditions) may have some limited influence on the results.
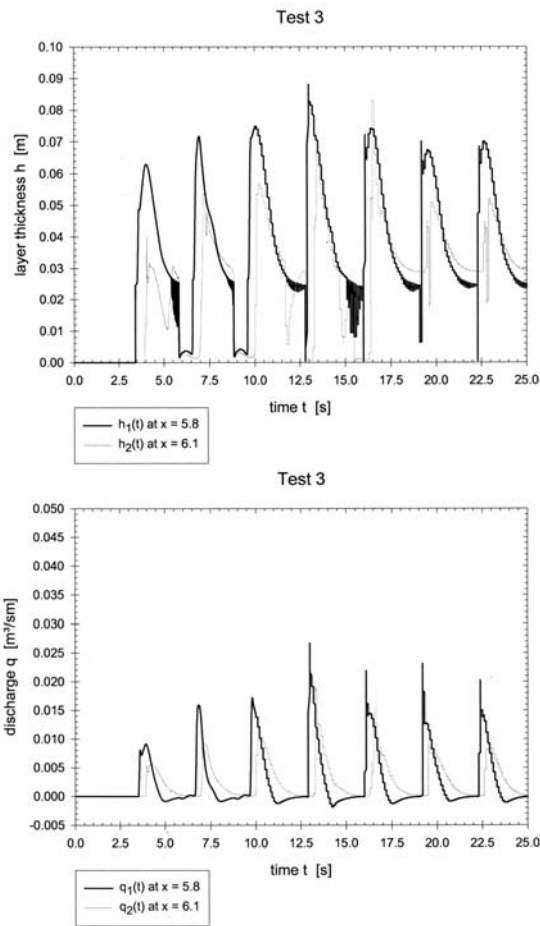
**Fig. 12.** *Time series of layer thickness* h(t) *and discharge* q(t) *at S1 and S2 for test 3.*

### 6.2.3 Cumulative volume V(t) and average overtopping rate $q_{num}$

The cumulative volume $V$ of overtopped water at both sections is calculated from $q(t)$, and is given in Fig. 13 for test 3. It is observed that a regular pattern of the wave overtopping in section S1 is present again. The cumulative overtopping volume in section S2 is time shifted (time required for the water to propagate over the crest), and seems to underestimate slightly the recorded overtopping volume in section S1. Seven individual overtopping events are present. The cumulative volume of water increases first and decreases slightly afterwards, during one wave period. This effect is due to the negative values of the discharge (in Fig. 12) meaning that water is flowing in the negative (i.e. seaward) direction at the start of the run-down.
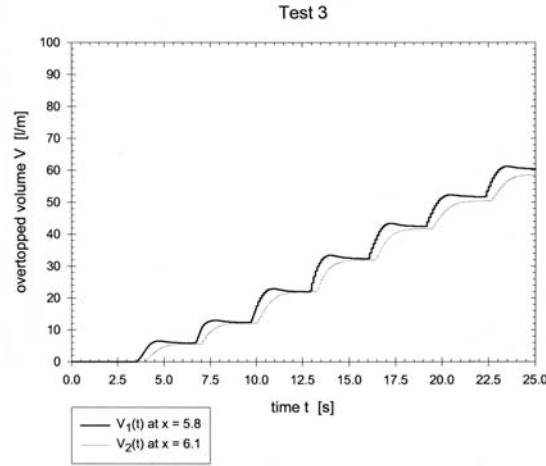
**Fig. 13.** *Time series of cumulative volume of overtopped water* $V(t)$ *at S1 and S2, for test 3.*

The average overtopping rate $q_{num}$ for test 3 is calculated from Fig. 13 as:

$$\frac{\Delta V}{\Delta t} = \frac{52.3 - 6.36}{22.4 - 6.74} = 2.93 \; 1/sm \qquad (6)$$

where the time interval is chosen from the start of the second overtopping event till the end of the sixth overtopping event. This result is averaged over 5 individual waves exhibiting a regular wave overtopping process. The average overtopping rate $q_{num}$ has been calculated in this way for all tests. Results have been summarised in Table 2.

The numerically obtained average overtopping rates $q_{num}$ are compared to the average overtopping rates $q_{lab}$ obtained from the physical model tests, for all tests (Table 2). Comparing both $q_{lab}$ and $q_{num}$, it is clear that there is an underestimation of the discharges in the numerical model. The underestimation ranges from $q_{num}/q_{lab} = 0.30$ for small overtopping volumes, till $q_{num}/q_{lab} = 0.71$ for large overtopping volumes. The deviation is largest for small q values and decreases for larger q values. However the relative magnitude of the discharges remains the same for all tests. This is shown in Fig. 14, where the tests are sorted from small $q_{lab}$ - values towards high $q_{lab}$ - values. The same ranking is found for the numerically obtained $q_{num}$ - values, proving that the numerical results contain the logical physical behaviour and that the deviations are consistent, and not random. Taking into account the scatter present in obtaining the measurements of the overtopping volumes in the physical model, it is concluded that there is a good agreement between physical model tests and numerical simulations.

**Table 2.** Average overtopping rates for numerical simulations ($q_{num}$) and for physical model tests ($q_{lab}$).

| $\xi_0$ | $q_{lab}$ | $q_{num}$ | $q_{num}/q_{lab}$ |
|---------|-----------|-----------|-------------------|

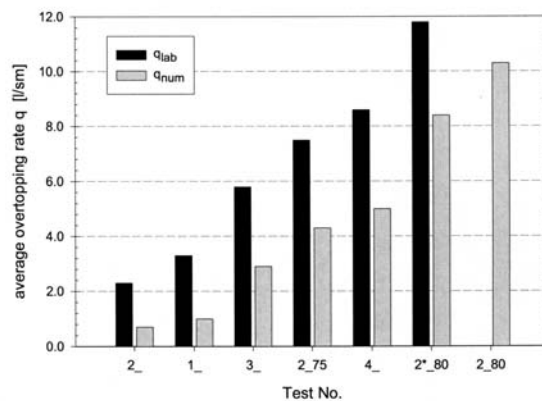| | Test No. | [-] | [l/sm] | [l/sm] | [-] |
|---|---|---|---|---|---|
| 1 | **1** | 1.0 | 3.33 | 1.0 | 0.30 |
| 2 | **2** | 1.5 | 2.32 | 0.7 | 0.30 |
| 3 | **3** | 1.9 | 5.79 | 2.9 | 0.50 |
| 4 | **4** | 2.5 | 8.59 | 5.0 | 0.58 |
| 5 | **2_75** | 1.5 | 7.51 | 4.3 | 0.57 |
| 6 | **2_80** | 1.5 | - | 10.3 | - |
| 7 | **2*_80** | 1.8 | 11.82 | 8.4 | 0.71 |



**Fig. 14.** *Tests with average overtopping values* $q_{lab}$ *from physical model tests sorted from small towards high values, and corresponding numerically obtained average overtopping values* $q_{num}$.

From an additional simulation, it is concluded that the choice of the computational grid is critical in obtaining good agreement with physical measurements, and that a lot of attention has to be paid to the definition of the grid. It is believed that even better agreement can be obtained by continuing the modifications (i.e. fine-tuning) of the grid.

## 5 Conclusions

The numerical model VOFbreak$^2$ has been presented for the simulation of wave interaction with two types of coastal structures, a rubble mound breakwater and a sea dike. The code is a numerical wave flume capable of simulating wave propagation and structural response in the vertical plane (2D). The range of applications that can be studied is broad, however this type of code requires considerable cpu-time for a single simulation (typically between 4 and 12 hours). The model is rather complex and only experienced users will be able to use it with adequate accuracy in the results. Therefore this type of code is mainly applicable for research purposes, and for complicated consultancy questions.

The pore pressure attenuation inside the Zeebrugge breakwater has been studied in the numerical wave flume VOFbreak$^2$. The successful validation of the wave interaction with a

breakwater with simple geometry has been presented. The Zeebrugge breakwater has been modelled in the numerical wave flume. Several types of results derived from the calculated variables have been presented, and are useful for further interpretation of the wave interaction. Comparing the numerically obtained pore pressures to the experimentally obtained conclusions, the same conclusions on the pore pressure distribution have been found.

Measurements from physical model tests of wave overtopping on a smooth impermeable sea dike have been used to validate the VOFbreak[2] numerical model for this type of wave-structure interaction. A dike geometry with a 1:6 outer slope has been used for the simulations, and a test programme including 9 simulations was executed. Overtopping quantities, such as layer thickness, discharge and cumulative volume of overtopping water have been calculated from the simulations. The resulting average overtopping rates have been derived, and compared to the average overtopping rates obtained in the physical model tests. Wave run-up and overtopping are modelled in a realistic way. A quantitative comparison of the results from the simulations and the physical model tests show good agreements for the average overtopping rates. This agreement is better for higher overtopping volumes. Finally it is indicated that the results are dependent on the grid definition.

With regard to future developments of the numerical wave flume, a number of important aspects have to be looked at, and are currently under development. For a better simulation of the wave breaking process, a state-of-the-art turbulence model will be implemented. Improvements with regard to the VOF method, the discretisation in finite volumes and the use of higher order discretisation schemes are underway. Validation of the code for the case of wave impact against vertical and horizontal walls is carried out.

## References

De Groot M.B., Yamazaki H., van Gent M.R.A., Kheyruri Z., 1994. Pore pressures in rubble mound breakwaters. Proc. 24th Int. Conference on Coastal Engineering, Kobe, Japan. ASCE, New York, Vol. 2, pp 1727-1738.

Harlow E.H., 1980. Large rubble mound breakwater failures. Proc. ASCE Jo. W'way, Port and Coastal Div., Vol. 106, WW2.

Kothe D.B., Mjolsness R.C., Torrey M.D., 1991. RIPPLE: a computer program for incompressible flow with free surfaces. Report LA-12007-MS, Los Alamos Scientific Report, Los Alamos, New Mexico, USA.

Nichols B.D., Hirt C.W., Hotchkiss R.S, 1980. SOLA-VOF: a solution algorithm for transient fluid flow with multiple free boundaries. Report LA-8355, Los Alamos, California, USA.

Oumeraci H., Schüttrumpf H., Bleck M., 1999. Wave overtopping at sea dikes. Comparison of physical model tests and numerical computations. OPTICREST technical report Task 3.2 and Task 5.

Troch P., 2000. Experimental study and numerical simulation of wave interaction with rubble mound breakwaters. Ph.D. thesis, Dept. Of Civil Engineering, Ghent University, Belgium.

Troch P., De Rouck J., 1999. An active wave generating-absorbing boundary condition for VOF type numerical model. Coastal Engineering, Vol. 38 (4), pp. 223-247.

Troch P., De Rouck J., Burcharth H.F., 2002. Experimental study and numerical modelling of wave induced pore pressure attenuation inside a rubble mound breakwater. 28th International Conference on Coastal Engineering, 7 – 12 July 2002, Cardiff, Wales (UK).

Troch P., De Rouck J., Schüttrumpf H., 2002. Numerical simulation of wave overtopping over a smooth impermeable sea dike. Proc. Advances in Fluid Mechanics AFM2002, Ghent, Belgium, pp. 715 – 724.